6-2021

Neutron Pulse-Time Extension through Conversion to Positronium

Shawn T. McTaggart

Neutron Pulse-Time Extension Through Conversion To Positronium

THESIS

Shawn Thomas McTaggart

AFIT-ENP-MS-21-J-031

DEPARTMENT OF THE AIR FORCE
AIR UNIVERSITY

AIR FORCE INSTITUTE OF TECHNOLOGY

Wright-Patterson Air Force Base, Ohio

AFIT-ENP-MS-21-J-031

Neutron Pulse-Time Extension Through Conversion To Positronium

THESIS

Presented to the Faculty

Department of Engineering Physics

Graduate School of Engineering and Management

Air Force Institute of Technology

Air University

Air Education and Training Command

in Partial Fulfillment of the Requirements for the

Degree of Master of Science in Applied Physics

Shawn Thomas McTaggart, B.S., Physics

June 17, 2021

AFIT-ENP-MS-21-J-031

Neutron Pulse-Time Extension Through Conversion To Positronium

THESIS

Shawn Thomas McTaggart, B.S., Physics

Committee Membership:

Larry W. Burggraf, Ph.D
Chair

Joshua R. Machacek, Ph.D
Member

Andrew J. Terzouli, Ph.D
Member

Abstract

Laser-Plasma Interactions have strong potential as future neutron sources. Measuring the neutron rate is difficult due to several issues: the very short duration of the laser pulse and subsequent fusion events (on the order of a few picoseconds), the corresponding short duration of the neutron pulse, and the simultaneous emission of other ionizing particles such as protons and electrons. Discussed here is a system to measure neutron emission by imposing a delay from the the emission of other radiation by conversion of the neutrons into ortho-positronium (o-Ps), the triplet state of positronium. Ortho-positronium has a long lifetime against annihilation of up to 142 nanoseconds compared to the picosecond lengths of these laser-plasma interactions. This lifetime extension enables more sensitive and selective detection of neutron pulses by time separation of the neutron component from other background signals that are correlated with laser-plasma interactions. This approach involves sequential steps including the thermalization of the neutrons, neutron capture and subsequent gamma emission, pair production, and the formation of positronium; thereby creating a delay in the signal that is dependent on the incident neutrons. Detection of o-Ps annihilation is accomplished with techniques developed for Positron Annihilation Lifetime Spectroscopy (PALS).

Table of Contents

List of Figures

List of Tables

Acknowledgements

This work was made possible thanks to our sponsor

Air Force Research Laboratory/RIT Paul F. Gilgallon, Principal Engineer, NCCC Systems and Technology Lead 523 Brooks Road Rome, NY 13441

My committee was invaluable in helping me understand and build this project, as was the entirety of AFIT's Nuclear Engineering department faculty and staff.

I would also like to acknowledge my family, whose constant support allowed me the time and peace of mind to execute this project.

Shawn Thomas McTaggart

Neutron Pulse-Time Extension Through Conversion To Positronium

I. Introduction

1.1 Statement of the Problem

High Altitude Nuclear Events (HANE) can cause disruption to SATCOM links by increasing scintillation [1]. While the most severe SATCOM disruption is caused by the gamma-ray burst from a HANE, this component is short lived [2]. Beta decay of the lower-energy fission neutrons, however, can cause long-lasting increases in the electron density [2], and thus have a strong effect on scintillation over a prolonged period.

Studying RF propagation through these environments is difficult, as above-ground nuclear testing has been banned by several treaties. Studying RF propagation in newer laser-induced plasmas and laser fusion experiments could serve as a proxy, if we could first characterize those environments better.

Powerful, fast lasers with ultra-intense pulses and high repitition rates are being used in the study of laser-plasma interactions (LPI)[3] [4]. The LPI can generate neutron pulses through acceleration of protons and ions to high energies to produce neutrons in deuterated material targets [5]. The nature of ion acceleration in LPI environments is still being investigated, with the idea of target-normal sheath acceleration (TNSA) losing ground to the newer idea of BreakOut Afterburner (BOA) ion acceleration [4]. Resultant neutron pulses can be as short as a few picoseconds. In laser-accelerated proton beam targets such as deuterated plastic, neutron flux as high as $10^{19}/(\mathrm{cm}^2\ \mathrm{s})$ have been reported from distances of a few millimeters from the

target [5].

The short temporal width of the neutron pulse can induce pulse pileup even in fast detectors as the response time is much longer than the neutron pulse. Neutron flux measurement in such a short time is difficult if the neutrons are not mono-energetic. The mixed background of charged particles from the LPI also complicates neutron detection, with protons and electrons emitted from the target area also being incident on the detector. The electron and proton energies can be in the MeV range and higher [5] [3].

Multi-step neutron conversion can be used to lengthen the detection window and decrease detector saturation by conversion of neutrons to positronium (Ps), a bound state of an electron and positron. Ortho-positronium, the triplet spin state of Ps, has characteristic vacuum lifetime of 142 nanoseconds. By moderating the neutrons, neutron capture in cadmium can be used to create gamma rays; gamma rays can be used to induce pair production in high-Z materials such as platinum or gold; and positrons can form positronium in porous materials such as aerogel by capturing electrons from ionized molecules in the medium and binding with the liberated electrons. Highly porous materials will increase the ortho-positronium production fraction and bulk lifetime, with material-dependent ortho-positronium lifetimes on the order of 50 nanoseconds. This will create a time delay in the signal from the initial LPI-induced neutrons.

1.2 Research Objectives

The primary goal of this research is to design a detection method to investigate neutron conversion for use in diagnostics for Laser-Plasma Interaction environments. Specifically, this project set out to find:

* The initial flux of neutrons incident upon the conversion system for an AmBe

test source

* The length of polyethylene for optimum neutron capture in ^{113}Cd

* The flux and delay time of the neutron pulse after moderation in polyethylene

* The gamma-ray flux and spectrum from neutron capture in ^{113}Cd

* The efficiency of pair production in platinum or gold foils from the incident gamma flux

* The positron flux and energies delivered to the aerogel absorber

* The absorption rate of positrons in the aerogel absorber

* The expected detection rate for the conversion system geometry of the 511 keV annihilation gammas from ortho-positronium decay

Simulations were performed to optimize and evaluate Neutron-to-Positronium conversion for commercially available materials. An experiment was designed using an AmBe source for validation, and the efficiency of the neutron-to-positronium conversion system was estimated based on a combination of simulations and calculations.

1.3 Document Overview

This document is organized as follows. Chapter II provides an overview of relevant background information for Positronium formation and detection, and some of the architecture of the designed system. Chapter III details the steps of the neutron-to-positron conversion. Chapter IV goes more in depth into these steps with calculated results from simulations. Finally, Chapter V discusses the conclusions drawn from the results and future experimental work to validate this method.

II. Background and Literature Review

2.1 Positronium

Positronium is a hydrogenic atom formed without nucleons by the binding of a positron and an electron. The vacuum lifetime of the triplet state of Ps, known as ortho-positronium (o-Ps) is 142 nanoseconds [6]. Positronium also forms in the singlet state, known as para-positronium (p-Ps), which has a lifetime of 125 picoseconds [6]. Para-positronium is usually detected as a prompt component due to this short lifetime and the detector impulse response time.

For this project, positrons are supplied for the formation of positronium by pair production. Pair production is a process by which gamma rays over a threshold energy of $2m_ec^2$ (1.022 MeV) can transfer their energy into the creation of a positron-electron pair by conservation of momentum [7].

Energetic positrons implanted into solid materials will ionize the molecules in the material as they pass into and through it, creating free electrons in the wake of the positron track through the material and decreasing the kinetic energy of the positron via inelastic collisions [8]. As the positron's kinetic energy is decreased though these events, the distance between these ionization events also decreases [8]. At lower kinetic energies, the positron experiences more diffusion and its momentum changes direction often due to elastic scattering and ionizations [8], causing ionizations to be localized in the proximity of the theralization. The localization of the ionizations is called a blob. As the positron energy decreases to a sub-ionizing level, it can become trapped in this blob, known as the terminal blob. This process is shown in Figure 1 [9].

Ortho-positronium cannot annihilate except via 3-photon annihilation in a pore, but can annihilate via pickoff with electrons during near collisions with pore walls [8].

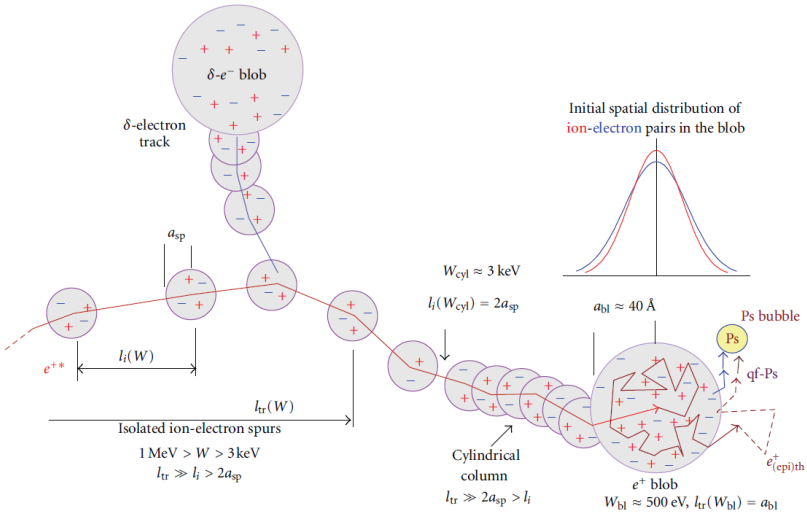

Figure 1: Positron track as it passes through materials, leaving a wake of ionizations, creating a blob, and forming Ps [9], used with permission

Pickoff annihilation is the result of the Ps wavefunction overlapping with the electron cloud of molecules at pore walls [10], allowing annihilation via electron exchange. A basic diagram (adapted from [11]) of this is shown in Figure 2, with ΔR as the overlap region. This creates a repulsive exchange force between the Ps atom and pore wall molecules; this force is balanced by van der Waals forces between the surface molecules themselves and as well as between the Ps atom and the surface molecules [10]. This creates a potential well that confines the Ps atom to the spaces between molecules in material voids, or pores [8] [10]. This is the basis for the Tao-Eldrup model [**?**]. The annihilation lifetime against pickoff in materials can be used to estimate the size of the voids, as shown in equation (1) [12].

$$\lambda_{\mathbf{TE}}(\mathbf{R}) = \lambda_{\mathbf{A}}[\mathbf{1} - \frac{\mathbf{R}}{\mathbf{R} + \mathbf{\Delta R}} + \frac{\mathbf{1}}{\mathbf{2\pi}}\mathbf{sin}(\frac{\mathbf{2\pi R}}{\mathbf{R} + \mathbf{\Delta R}})]. \tag{1}$$

The formulation of equation (1) uses values for the decay rate of annihilation of a free positron in the electron cloud (λ_A, approximately 2 nanoseconds), the pore radius R, the overlap radius of the Ps wavefunction (ΔR, experimentally measured

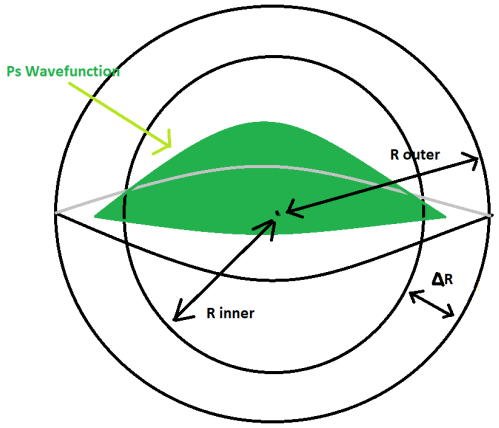

Figure 2: Ps wavefunction overlap with molecular electrons over the range ΔR, adapted from [11]

to be 0.165 nanometers [12]). λ_{TE} is the decay rate of the pickoff annihilation.

Ps formation in porous SiO_2 has been studied by positron annihilation lifetime spectroscopy (PALS) to examine pore size, and found to occur with high probability [8]. This makes aerogel (a highly porous form of SiO_2) a highly desirable target medium for positrons to create localized Ps atoms.

2.2 pyPenelope Transport Code

Positron creation fractions were calculated from pyPenelope simulations. This code is a front-end user interface for PENELOPE [13]. PENELOPE is an acronym for PENetration and Energy LOss of Positrons and Electrons, the name owing to it's creation before the inclusion of photon transport. This is a Monte Carlo code that models photon, electron, and positron transport through and interactions within materials in it's database.

The Monte Carlo code implements random path lengths for the modeled particle at each step, up to a maximum step length. Then it uses a combination of numerical databases and analytical cross-sections to determine the probabilities of interactions

between the particle and the material over the step length. The energy range of the particles it can model is from a couple hundred eV to about 1 GeV [13].

Electron and positron transport is simulated step-by-step for interactions that result in a scattering angle θ_c or energy loss W_c less than a set cutoff quantity [13]. The default value can be used, or can be set by the user. In this project, default values were used. For scattering angles and energy losses less than these cutoff values, PENELOPE uses multiple scattering approaches to save computation time.

For photons, PENELOPE can implement the following interactions:

* Photoelectric effect

* Coherent (Rayleigh) scattering

* Incoherent (Compton) scattering

* Electron-positron pair production

* Attenuation

* Atomic relaxation

* Polarized photon scattering

These interactions are modeled based on the differential cross-sections for their interaction type, from databases such as LLNL Evaluated Photon Data Library, and XCOM [14] [15].

For positrons and electrons, the following interactions can be implemented by PENELOPE:

* Elastic collisons

* Inelastic collisions

* Bremsstrahlung emission

* Positron annihilation

These interactions are based on a large variety of analytical models described in [13].

2.3 Positron Annihilation Lifetime Spectroscopy

Detection of the decay of positronium is the basis of Positron Annihilation Lifetime Spectroscopy (PALS) and Single-Shot PALS (SSPALS). The lifetime of positrons travelling through a medium is changed by positronium formation, and positronium lifetimes are highly dependent on the pore sizes of the material it forms in. This makes PALS a useful diagnostic tool for the sizes of pores and lattice defects in materials. An example SSPALS spectrum is shown in Figure 3 [16].

The vacuum lifetime of o-Ps is the maximum lifetime seen in PALS and SSPALS experiments [17]. Electron exchange converts o-Ps to p-Ps in materials and consequently causes lifetimes in the tens of nanoseconds [16]. In PALS experiments, a detector with a fast rise time is sufficient, but for SSPALS, measurement of the annihilation lifetime requires a detector with a fast, single component response owing to the large number of annihilation events in each shot. Typically, $PbWO_4$ (lead

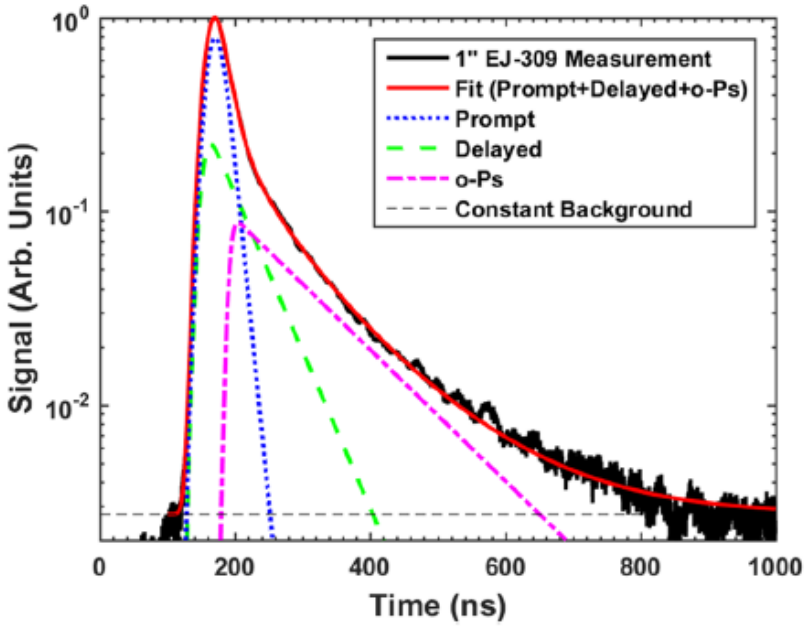

Figure 3: SSPALS spectrum of stainless steel, created with AFIT's positron beam, and captured with an EJ-309 liquid scintillator [16]

tungstate) and LYSO (lutetium yttrium oxyorthosilicate) detectors are used in SSPALS work due to their fast response time [4]. Recently, use of the EJ-309 liquid scintillator was investigated and shown to be sufficient for use in SSPALS and positronium lifetime measurements [16] by a group including this author as a demonstation of this project. The EJ-309 has a fast response time of 3.5 nanoseconds [18], which is fast enough to measure even o-Ps lifetimes that have been significantly curtailed by pickoff annihilation. The pulse shape discrimination ability of the EJ-309 makes it ideal for use in mixed gamma and neutron environments [18], such as this conversion system will create.

2.4 Neutron Conversion

Positrons are supplied for Ps formation by pair production from gamma rays produced in neutron capture. The technique used in this project was adapted from that used in conjunction with the high flux reactor at the ILL in Grenoble to create a high-intensity positron beam [19]. That setup uses the high neutron flux created in the reactor and several steps to create a positron beam with an intensity of 3 X 10^4 positrons per second and a beam diameter of 20 mm [19]. A cold neutron flux of 3.39 X 10^9 neutrons per second per cm^2 is incident on a 1.5 mm cadmium foil. ^{113}Cd has a high capture cross-section of 6.46 X 10^4 barns for the target neutron energy of 0.178 eV. Gamma rays released from the $^{113}Cd(n,\gamma)^{114}Cd$ reaction trigger pair production in a series of 125-micron thick platinum foils, providing the positrons. This basic architecture has been proven for a variety of positron beams around the world [19][20].

III. Methodology

Preamble

The neutron conversion process consists of 5 steps: moderation of neutrons, neutron capture in cadmium, pair production in platinum (or gold) of gammas produced in cadmium neutron capture, positron thermalization followed by positronium formation in aerogel from positrons created in platinum (or gold), and decay of positronium in aerogel by annihilation. This is illustrated in Figures 4 and 5.

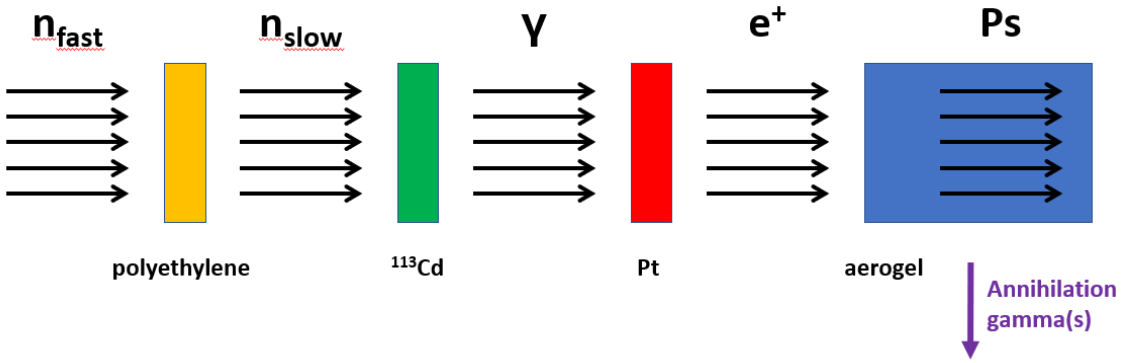

Figure 4: Overview Diagram of Neutron Conversion Process

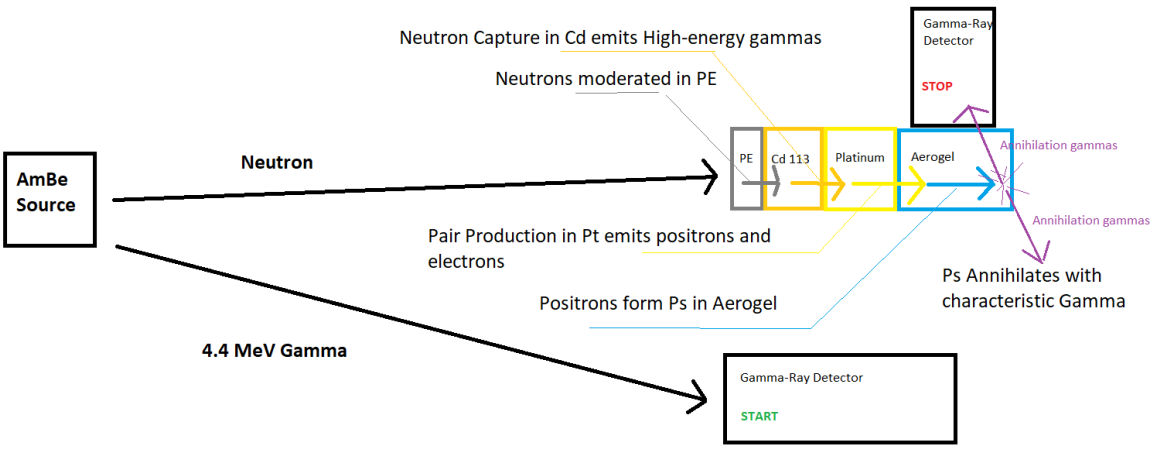

Figure 5: Step-by-step diagram of neutron conversion process

3.1 Neutron Source

Neutrons are created in the Americium-Beryllium (AmBe) source. Americium and Beryllium powders are placed in layers to provide intimate contact between the constituents [21]. Americium (^{241}Am) decays by alpha decay into Neptunium (^{237}Np), emitting an alpha particle and a 54.5409 keV gamma photon, as shown in equation (2) [22].

$$\mathbf{^{241}_{95}Am \rightarrow {}^{237}_{93}Np + {}^{4}_{2}\alpha + \gamma(59.5409keV)}. \tag{2}$$

Some of the emitted alpha particles are incident on the Beryllium (^{9}Be) atoms. These incident alpha particles are captured by the ^{9}Be, creating an excited Carbon (^{12}C*) atom and emitting a neutron as shown in equation (3) [22]. The ^{12}C* atom de-excites by emitting a 4.4 MeV gamma photon.

$$\mathbf{^{9}_{4}Be + {}^{4}_{2}\alpha + T_{\alpha} \rightarrow {}^{12}_{6}C^{*} + n + T_{n}}. \tag{3}$$

A typical AmBe source emits 70 neutrons per MBq of the source activity [22]. These neutrons are emitted with a spectrum of kinetic energies from 1-11 MeV, with 4.2 MeV being the most common, as shown in figure 6 [23].

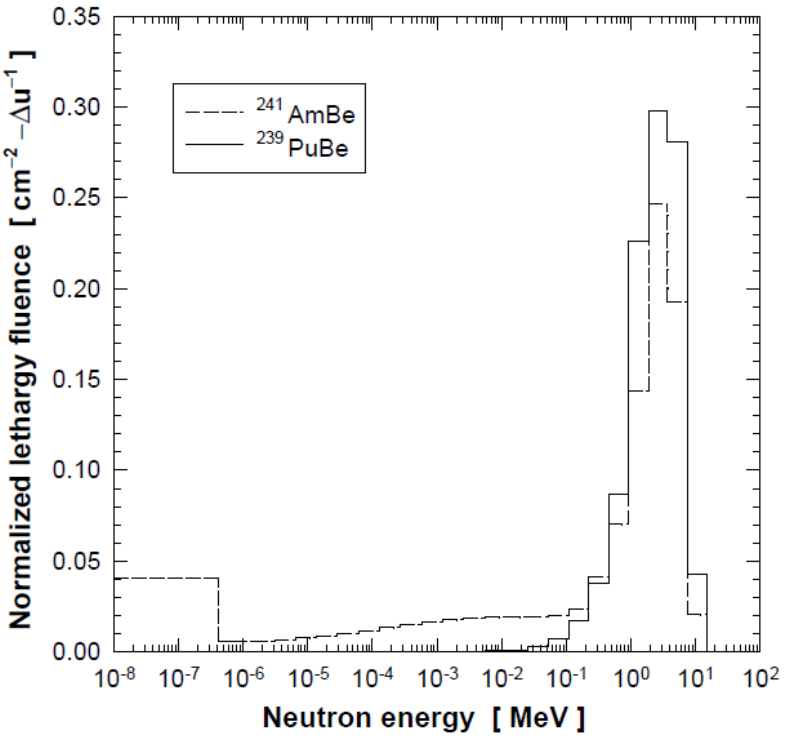

Figure 6: Neutron energy spectrum of AmBe and PuBe sources [23], used by permission

3.2 Polyethylene Moderation

Neutrons are moderated to access the high neutron capture cross-section in the cadmium (^{113}Cd). The peak in the neutron capture cross-section at 0.178 eV is the target kinetic energy for the moderated neutrons, as shown in figure 7 [24].

Polyethylene (PE) was used as the moderating material. To calculate the number of collisions necessary in PE to reach this target kinetic energy, the energy of a scattered neutron was calculated by equation 12.7 from [7],

$$\mathbf{lnE'_n = lnE_0 - n\zeta}, \tag{4}$$

where ζ is the lethargy of each atom, calculated by equation 12.8 from [7], shown in equation (5).

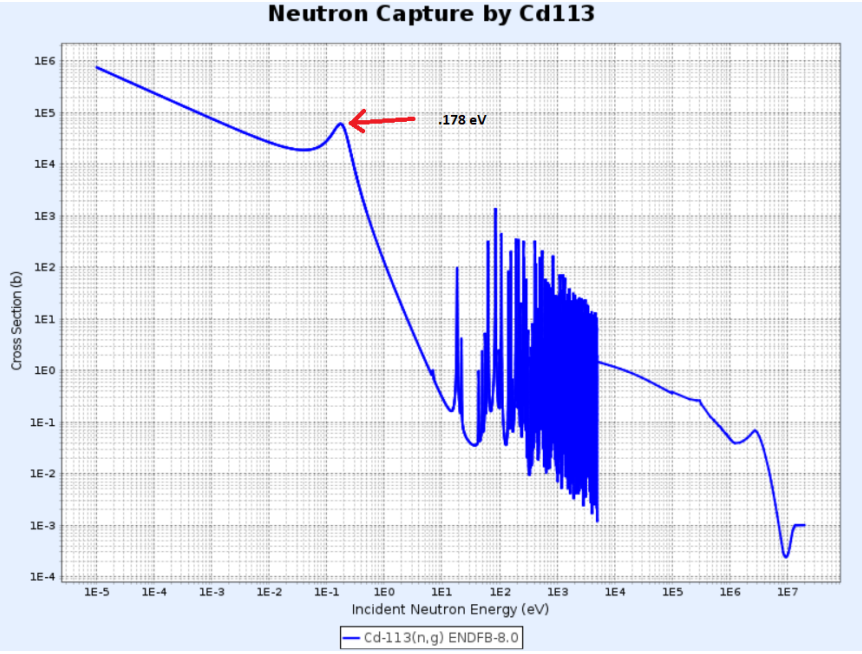

Figure 7: Neutron capture cross section in ^{113}Cd, with target kinetic energy highlighted [24]

$$\zeta = \mathbf{1} + \frac{\mathbf{(A-1)^2}}{\mathbf{2A}} \mathbf{ln}\left(\frac{\mathbf{A-1}}{\mathbf{A+1}}\right) \tag{5}$$

The polyethylene molecule's chemical formula is C_2H_4, with the hydrogen atoms shielding out many of the carbon atoms as shown in figure 8 [25]. Thus, hydrogen's lethargy of 1 [7] is used in the scattering calculation. This leads to a calculation that 17 collisions are necessary to reach the target kinetic energy of the neutron. As the neutron loses kinetic energy in each scattering event, the mean free path changes. The energy dependent mean free path for a neutron in PE is shown in Figure 9 [26]. Values estimated from Figure 9 were used to find the thickness of polyethylene needed to reach the target energy of 0.178 eV as 20.2 cm of PE. This led to a cacluated moderation time of about 330 μs as discussed in section IV.

The attenuation of the incident neutron energy by PE was calculated by equation (6):

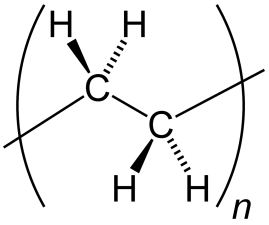

Figure 8: Characteristic structure of the polyethylene molecule [25], used with permission..

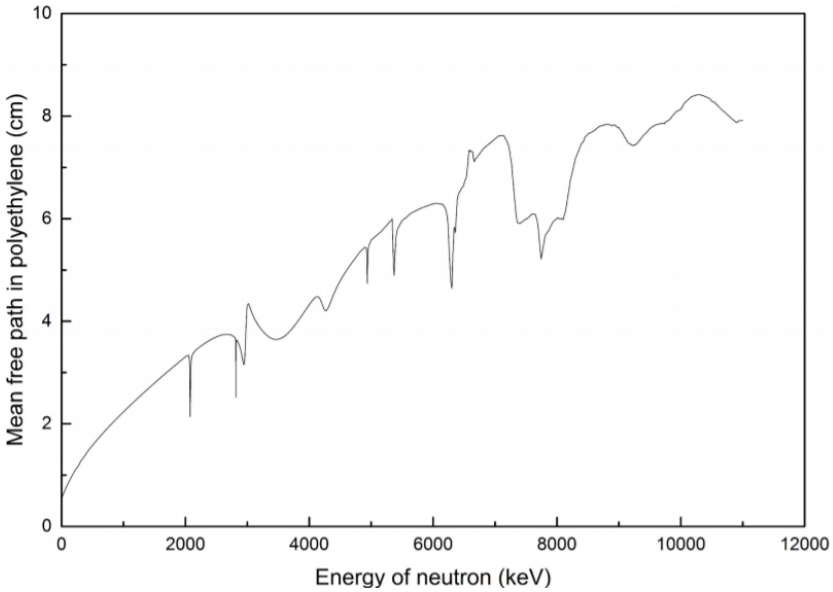

Figure 9: Mean Free Path of neutrons by energy in polyethylene [26], used with permission.

$$\mathbf{I_{n,exit} = I_0 e^{-\Sigma t}}, \tag{6}$$

with I_0 being the incident neutron flux, $I_{n,exit}$ being the neutron flux after attenuation in PE, and t being the thickness of the PE. The attenuation cross-section, Σ, was calculated by equation (7) [26]:

$$\mathbf{\Sigma = \frac{\rho N_a}{M}(2\sigma_C + 4\sigma_H)}, \tag{7}$$

where ρ is the density of PE, N_a is Avagadro's number, M is the molar mass of

PE, and σ_C and σ_H are the coherent scattering cross-sections for neutrons in carbon and hydrogen, respectively [24].

This leads to a neutron flux of 2.4 X 10^5 per second exiting the 20.2 cm thick polyethylene stage. This was calculated for an AmBe source with a typical activity of 7.49 X 10^{11} Bq [27], at a distance of 1 cm from the entrance to the PE.

3.3 Cadmium Neutron Capture

The moderated neutrons are incident on a 1.5mm thick slab of cadmium, as used in [19]. This leads to neutron capture in the cadmium 113, as shown in equation (8). The branching ratios for these decays were estimated from the graph in Figure 11 [28], and shown in Table 1.

$$\mathbf{^{113}_{48}Cd + n \rightarrow {}^{114}_{48}Cd^{*}} \tag{8}$$

3.4 Cadmium Gamma Emission

Neutron capture produces cadmium 114 in an excited state. The excited Cadmium 114 atoms relaxes to the ground state by emitting gamma rays. The energy level diagram of the excited cadmium 114 is shown in Figure 10.

Gamma ray flux incident on the platinum foil stage was calculated for each of the gamma energies produced from the relaxation of the excited Cadmium 114. Attenuation of the gamma rays, the natural abundance of Cadmium 113, and the solid angle of the emitted gammas were taken into account for this calculation. The total gamma flux was calculated to be 13771 gammas per second, although calculations from this step forward involved different fluxes for each of the respective gamma energies due to their branching ratios.

The attenuation of these produced gamma rays in the cadmium was calculated

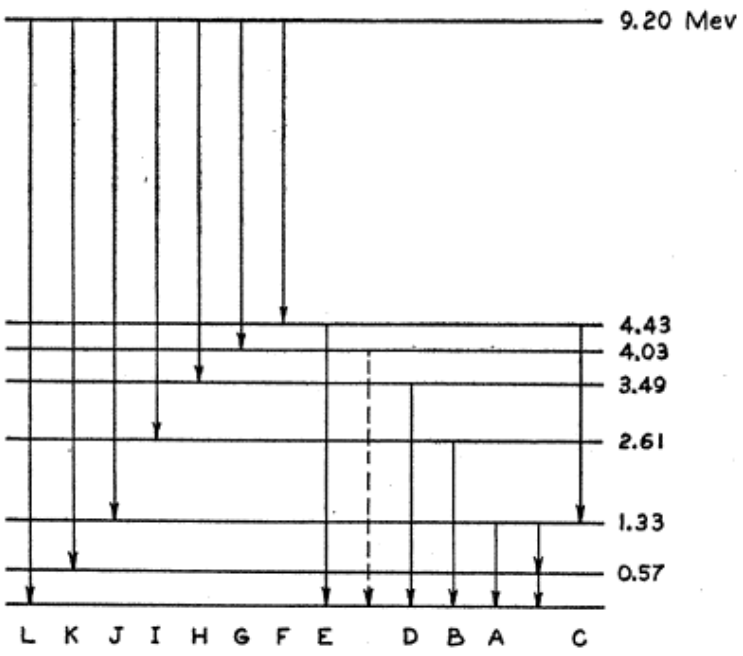

Figure 10: Cadmium 114 Level Structure with transition lengths [28], used with permission.

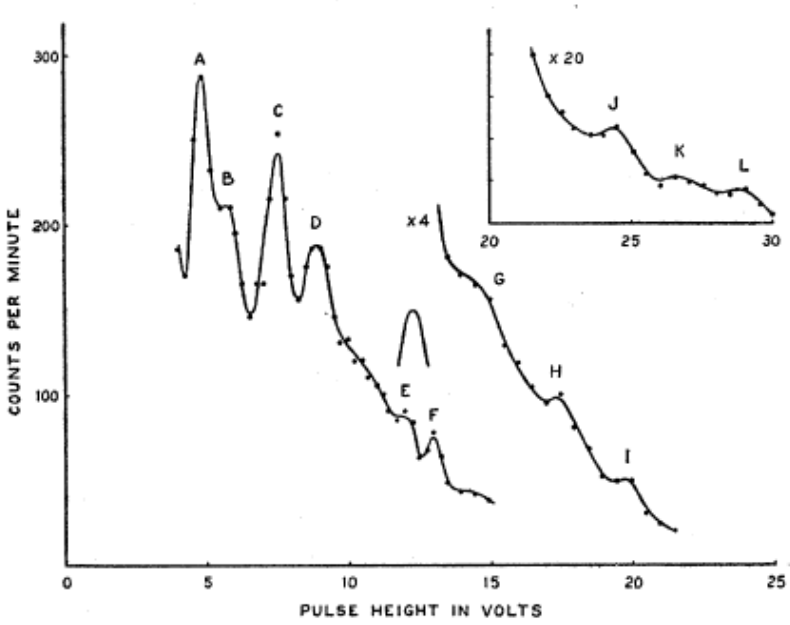

Figure 11: Normalized Counts per minute for various gamma-rays associated with neutron capture in ^{113}Cd [28], used with permission.

Table 1: ^{113}Cd neutron capture gammas and their branching ratios

Peak Label	**Counts per Minute**	**Energy, in MeV**	**Branching Ratio**
A	290	1.330	0.0242
B	220	2.610	0.0184
C	250	3.140	0.0209
D	190	3.490	0.0159
E	100	4.430	0.0084
F	85	4.710	0.0071
G	1000	5.170	0.0835
H	400	5.850	0.0334
I	240	6.610	0.020
J	4800	7.920	0.4008
K	2400	8.550	0.2004
L	2000	9.200	0.1670

by the mass-attenuation coefficients given by the NIST database [29] using equation (9).

$$\mathbf{f_\gamma = f_{\gamma 0} e^{-\rho_{Cd} \frac{\mu_{Cd}}{\rho_{Cd}} t}} \tag{9}$$

where f_γ is the gamma flux exiting the cadmium foil, $f_{\gamma 0}$ is the gamma production rate, ρ_{Cd} is the density of cadmium (in g/cm^3), μ_{Cd}/ρ_{Cd} is the mass attenuation coefficient of the cadmium at the individual gamma energies (in cm^2/g), and t is the thickness of the cadmium foil (in cm).

3.5 Platinum Pair Production

Pair production takes place in two 125-micron thick platinum foils, separated by 2.1 cm of aerogel. This creates positron-electron pairs within the platinum foil. The positrons from pair production are emitted from the platinum foils into the aerogel layers to promote the formation of positronium, which has a lifetime against annihilation of 10's of nanoseconds in this material.

The positron creation fractions calculated in pyPenelope simulations (see Background) was compared to the fraction that would be calculated using the pair production cross-sections available from NIST [14]. Linear interpolation was used to find the cross-section coefficients for the specific energies of the gammas from the cadmium neutron capture. The gamma ray attenuation from pair production was calculated by equation (10),

$$\mathbf{I_\gamma = I_{\gamma 0} e^{-\rho \sigma_{PP} t}}, \tag{10}$$

where $I_{\gamma 0}$ and I_γ are the incident and exit gamma flux, ρ is the density of platinum in cm^2 per gram, σ_{PP} are the energy dependent cross-sections for pair production in platinum, and t is the thickness of the platinum.

The pair production fraction from NIST was then calculated by equations (10) and (11).

$$\frac{\mathbf{I_{\gamma 0} - I_\gamma}}{\mathbf{I_{\gamma 0}}.} \tag{11}$$

This was compared to the fraction of the incident gammas that resulted in positrons in the pyPenelope [13] simulation, shown in Figure 12. While pyPenelope simulations show a greater positron production efficiency than is calculated by NIST pair-production cross-sections, the trends align.

Positrons are then absorbed in the aerogel, a fraction of which will form o-Ps. Modeling was carried out in pyPenelope to find the absorption positions. As positrons were created in both platinum foils, this was run as two separate simulations. The first simulation modeled positrons created in the first platinum foil and transported through the entire model. The second simulation modeled positrons created in the second platinum foil and transported through half the model. As the positrons created

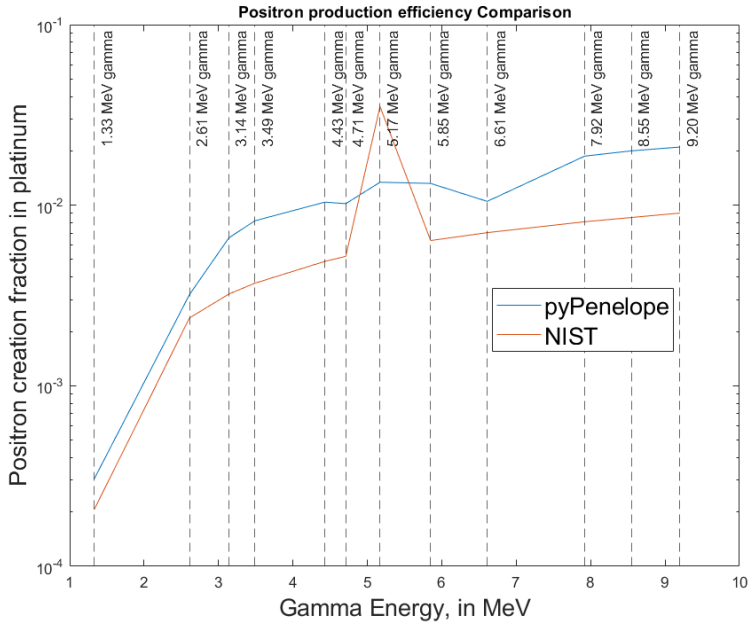

Figure 12: Comparison of pyPenelope and NIST positron production in 125-microns of Platinum.

in the second foil are emitted in all directions, these positrons will also be emitted back into the identical first half of the model, thus the results of the second simulation were doubled. The backscattering of the positrons by the foil was also used to calculate a few additional absorbed positrons. The results of these simulations are shown in Figures 13 and 14, respectively.

The gamma-to-absorbed-positron efficiency was calculated as the ratio of positrons absorbed in the aerogel to the number of incident gamma rays. A total of 1377090 gammas yielded 43 aerogel-absorbed positrons, for an efficiency of 0.00312% in these simulations.

Positrons transported through the platinum foil and absorbed in the aerogel layer will seek out voids in the material, and be trapped there. These positrons can then form positronium (Ps) in either the ortho or para state, with their respective 142 nanosecond and 125 picosecond lifetimes.

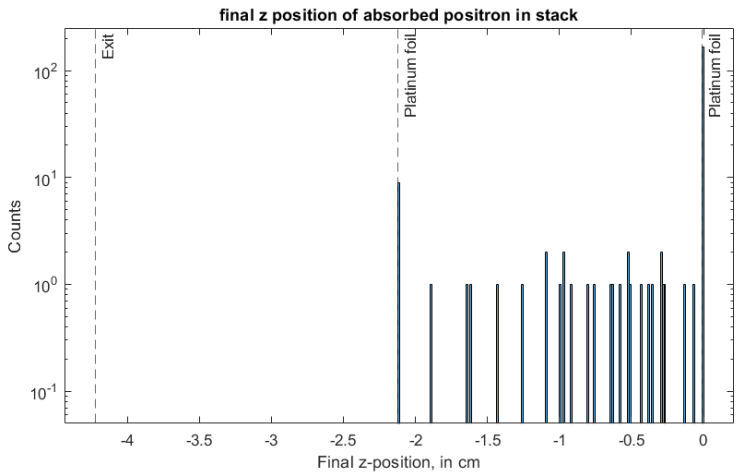

Figure 13: Positron Transport simulation for the whole model in pyPenelope.

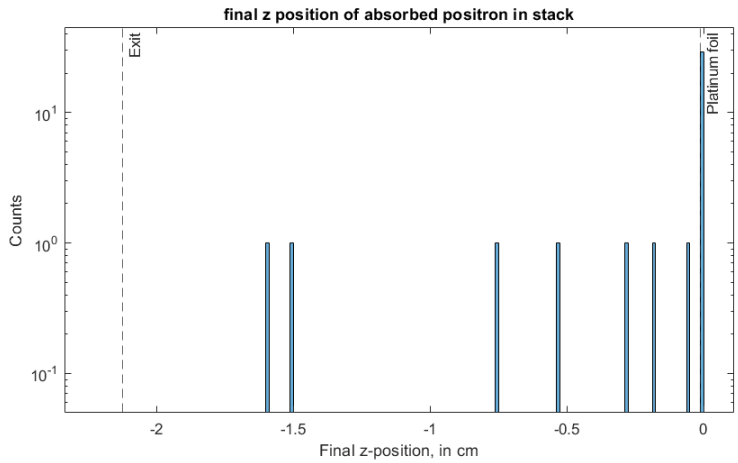

Figure 14: Positron Transport simulation for the second half of the model in pyPenelope.

Different aerogel compositions have been shown to have differing ortho-positronium creation fractions and lifetimes against pickoff annihilation. A list of some of these appears in [30]. For this project, the quoted 29% o-Ps fraction of Standard Cabot Aerogel and it's o-Ps lifetime of 58.8 seconds was chosen [30] as it is believed by the author to be the closest to the Hydrophobic Silica Aerogel discs to be used in validation experiments.

IV. Results and Analysis

Calculations and simulations were carried out to explore the concept of a neutron-to-positronium conversion scheme. This was done to gain a quantitative understanding of the parameters of the system in terms of the various particle fluxes at each layer, time delays introduced, and the overall conversion efficiency.

A proof-of-concept experiment was designed using an AmBe neutron source to determine viability. The Air Force Institute of Technology has neutron sources for detection research, one of which was an AmBe source. The activity of a typical AmBe source (749 GBq [27]) was used for calculations. An estimate of 70 neutrons per million ^{241}Am alpha decays [22] was used to calculate the neutron activity of the AmBe source. This led to a neutron production rate calculated to be 5.245 X 10^7 Bq.

As the conversion system has very low overall efficiency, it was decided to position the source only 1 cm from the entrance to the conversion system to increase neutron flux. The solid angle of the 6.25 cm^2 polyethylene surface and the neutron-specific source activity were used to calculate the flux of neutrons incident upon the PE surface at the 1 cm distance. This yielded a neutron flux at the PE surface of 2.6 X 10^7 neutrons per second.

Moderation makes the neutrons travel slower as they lose kinetic energy. This aids in the separation of the neutron signal from the particle background inherent in laser-plasma interactions. The velocity of the neutrons was calculated after each scattering event. Using these velocities in conjunction with their respective mean free paths, neutron time-of-flight (TOF) was calculated for transport through the PE moderator as 330 μs. The changing velocity of the neutrons as they pass through the PE is shown in Figure 15.

Next, calculations were performed to determine the thickness of PE needed to reach the target neutron kinetic energy of 0.178 eV for maximum neutron capture

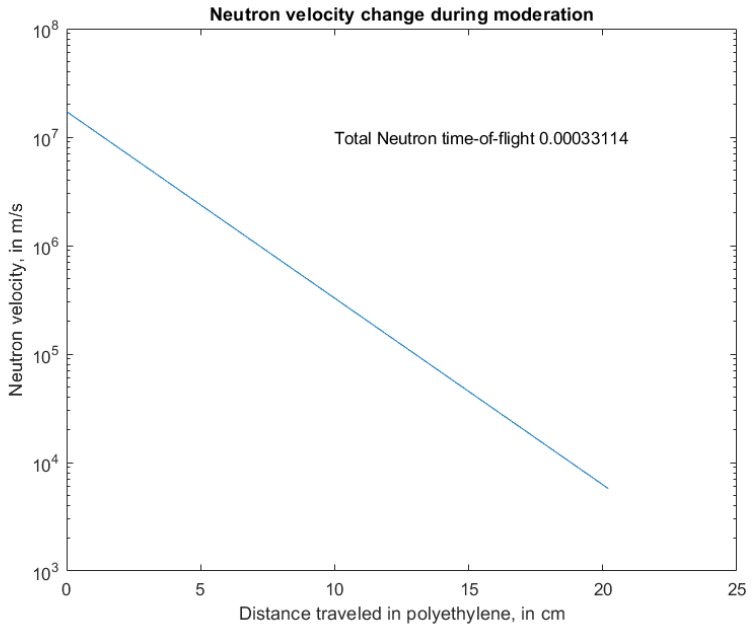

Figure 15: Neutron velocities after scattering events

in ^{113}Cd. The number of scattering events needed was calculated using equation (4) and a lethargy of 1 for the polyethylene [7], and the average kinetic energy of the neutrons from an AmBe source of 4.2 MeV [22]. This was calculated to be 16.97, or 17, scattering events. Using a graph of the neutron mean free path (MFP) in PE [26], the neutron kinetic energy was calculated by equation (4) after each scattering event. Then that neutron energy was matched to the MFP in the graph. All MFP's for each of the 17 scattering events were then summed to get the optimal thickness of PE to moderate neutron kinetic energy to the desired 0.178 eV. The result of this calculation was 20.2 cm of PE.

Once the moderator thickness was calculated, the total scattering cross-section of polyethylene was used to determine the attenuation of the neutron flux as it passed through the PE by equations (6) and (7). The total scattering cross-sections of the hydrogen and carbon atoms in the PE molecule used were given by the Nuclear Data Center at KAERI [24] for the target neutron kinetic energy of 0.178 eV. This led to

a calculation of 2.4 X 10^5 moderated neutrons per second exiting the PE moderator stage and being immediately incident upon the cadmium foil for neutron capture.

This neutron flux incident upon the cadmium foil was used to calculate the gamma ray flux from neutron capture in ^{113}Cd. The natural abundance of ^{113}Cd is 12.2%, which was taken into account in the gamma flux calculation. The cross-section for neutron capture in cadmium [24] was used to determine the attenuation of the neutron flux by neutron capture in the 1.5mm thick cadmium foil. This was subtracted from the incident neutron flux and multiplied by the natural abundance of ^{113}Cd to give the number of neutron capture events in the cadmium foil.

When neutron capture in ^{113}Cd occurs, the nucleus gains a neutron which results in the creation of an excited ^{114}Cd nucleus. The ^{114}Cd relaxes the excitation by gamma emission. Experimental observation of the relaxation of the excited ^{114}Cd [28] was used to estimate the branching ratios for the different energy gammas given off during de-excitation. Twelve different gammas are produced from this relaxation [28], shown with their respective branching ratios and production rate in Table 2.

Table 2: ^{113}Cd neutron capture gammas, their branching ratios, and production rates [28].

Gamma Energy, in MeV	**Branching Ratio**	**photons produced per second**
1.33	0.024	700
2.61	0.018	531
3.14	0.021	603
3.49	0.016	459
4.43	0.008	241
4.71	0.007	205
5.17	0.084	2414
5.85	0.033	966
6.61	0.020	579
7.92	0.401	11587
8.55	0.200	5793
9.20	0.167	4828

The calculated total gamma flux exiting the cadmium foil and incident on the platinum foil (summing over all of the gamma energies) is calculated by equation (9) to be 13771 gammas, accounting for a solid angle of the platinum of one half due to direct contact between the exit surface of the cadmium and the entrance surface of the platinum.

Positrons are created in the platinum foil via pair production from the incident gammas. This step was investigated by simulation in pyPenelope [13]. Incident gammas were simulated in twelve individual simulations in numbers proportional to the incident gamma rates calculated for each of the gamma energies. A model was constructed in pyPenelope with layers consisting of: a 125-micron thick platinum foil, followed by a 2.1 cm thick layer of aerogel (SiO_2 at a density of 0.1 g/cm^3), followed by a second 125-micron platinum layer, followed again by a second 2.1 cm aerogel layer. The simulated gamma transport in this model had 3 exit conditions: absorption, transmission, or backscattering.

The simulated gamma absorption data was analyzed to find the absorbed gammas whose final collision data indicated pair production. This data was collated with the final position of the gammas to find the positions of created positrons. Histograms for this data were created with respect to position for each gamma energy. The bin widths of these histograms were chosen to be the thickness of the platinum foils to be able to clearly separate the simulated positron creation in the platinum foils from those in created in the aerogel. The combined histogram of positron creation from all the simulated gamma energies is shown in Figure 16.

The positrons created in the platinum foils were counted for each energy and the quantity for each was used in later simulations of positron transport in the model. The simulations in pyPenelope showed higher pair production rates than those calculated by NIST, as shown in Figure 12, but the overall shape is consistent enough to use as

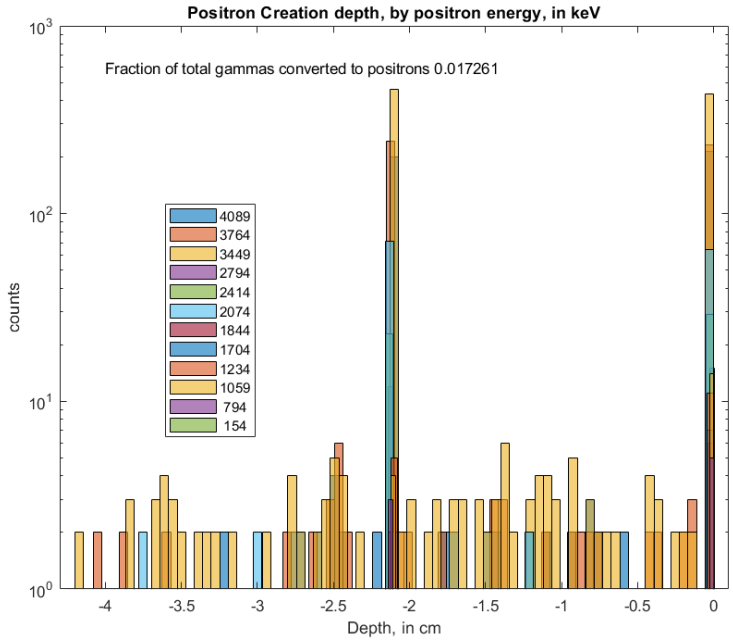

Figure 16: Positron creation in platinum calculated by pyPenelope simulations

a benchmark of the pyPenelope simulations.

The final energy of the gammas before pair production was also checked, but they so rarely varied from their initial energy that it was assumed that the initial gamma energy participating in the pair production process was the full energy of the incident gammas. Positron kinetic energies were then calculated by subtracting the rest mass of the positron-electron pair from the incident gamma energy and dividing the leftover energy by two, as shown in equation (12). This step assumes the positron-electron pair split the available kinetic energy evenly to simplify calculations.

$$\mathbf{T_+ = \frac{E_\gamma - 2mc^2}{2}} \tag{12}$$

The entire process was also simulated for a conversion system that replaced the platinum foils with gold foils of the same thickness. The histogram for positron creation in this simulation is shown in figure 17.

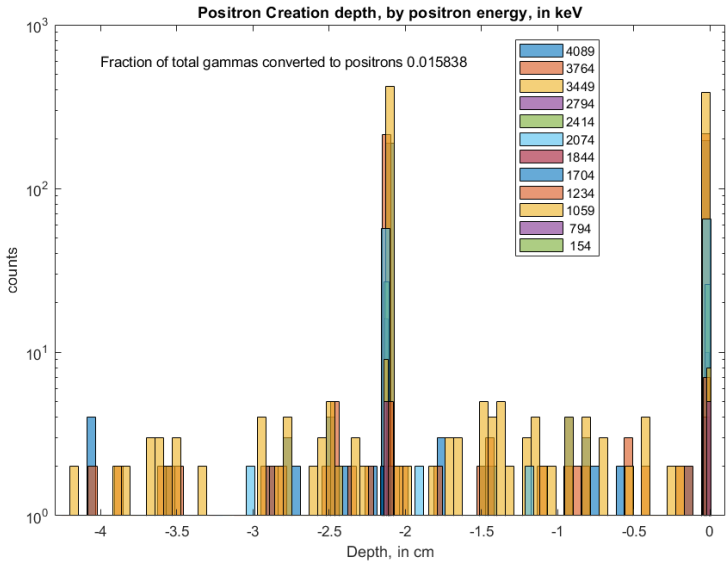

Figure 17: Positron creation in gold calculated by pyPenelope simulations

Platinum showed a better ratio of positron creation at 1.72% vs. the ratio in Gold of 1.58%.

Transport for the created positrons in either model was then calculated by simulations of each of the twelve positron kinetic energies. The number of positrons in each simulation was proportional to the number of each energy that led to a pair production event in the platinum foils from the previous simulation. Positron transport simulations for each material were carried out in two steps. The first simulated the positrons created in the first foil, and the simulation used an identical model to the pair production simulations. The final position of these absorbed positrons for platinum is shown in the previous figures 13 and 14.

The positrons absorbed in the aerogel layers (between the foils) were counted for each simulation, but the counts in the second simulation were doubled to account for positrons being emitted in both directions from the foil. The backscattering fraction of each positron energy was also applied to the absorbed positrons counted for that energy, and added to the total. This resulted in 43 positrons absorbed

in the aerogel layers for the platinum foil model from 1377090 incident gammas, for a 0.00312% gamma-to-absorbed-positron efficiency. For the gold foil model, 80 positrons were absorbed in the aerogel layers from 1377090 incident gammas, for a 0.00581% efficiency.

While simulations using a platinum foil showed better pair production efficiency, simulations using the gold foil showed better positron absorption efficiency in the aerogel layers. Total positron absorption rate in the aerogel was calculated by taking the incident gamma flux on the foils and multiplying it by the gamma-to-absorbed-positron efficiency from the pyPenelope simulations. The total positron absorption rate for the conversion system using platinum foils was 0.43 absorbed positrons per second, while the rate using the gold foils was 0.80 absorbed positrons per second.

Positronium creation in aerogel has been experimentally measured [30]. See [30] for the o-Ps fractions and lifetimes measured in that study.

For calculations, the Standard Cabot Aerogel o-Ps fraction was used. An EJ-309 liquid scintillator was used for detection of positronium decay. The efficiency of this detector with a typical 511 keV annihilation gamma is 29% [31], shown in Figure 18. The solid angle of a 3" EJ-309 put directly up against this conversion system was calculated to be 0.4306 steradians. These values were used to calculate a counting rate of annihilation gammas from o-Ps of 0.0156 per second in the platinum foil system, and 0.0290 per second in the gold foil system. Shown in table 3 are calculated count times needed to reach different count totals for o-Ps for this scheme.

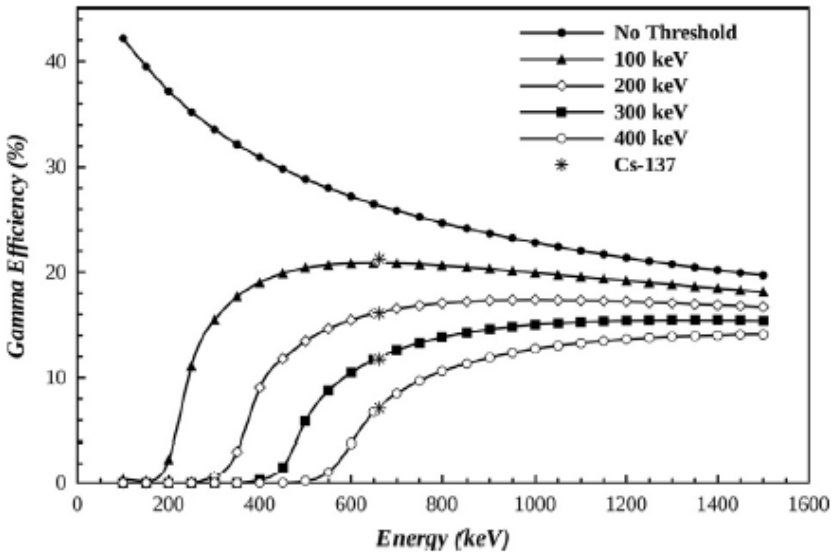

Figure 18: Gamma Detection Efficiency of the EJ-309 [31], used with permission.

Table 3: ^{113}Cd neutron capture gammas and their branching ratios

type	**Total Counts**	**Days**	**Hours**
$125\mu mPt$	1×10^6	473.360	17841
$125\mu mPt$	1×10^5	74.336	1784.1
$125\mu mPt$	1×10^4	7.434	178.41
$125\mu mPt$	1×10^3	0.743	17384
$125\mu mAu$	1×10^6	399.550	9589
$125\mu mAu$	1×10^5	39.960	958.9
$125\mu mAu$	1×10^4	3.996	95.89
$125\mu mAu$	1×10^3	0.400	9.589

V. Conclusions

The overall conversion process has a calculated efficiency for detection of 6 X 10^{-10} for a given neutron source, independent of souce activity. The polyethylene thickness needed was calculated by means of the energy-dependent mean free path of neutrons in polyethylene (PE). The neutron intensity attenuation was calculated for this length of PE. The rate of gamma production in cadmium for the various gamma energies associated with neutron capture in ^{113}Cd and their attenuation through the bulk of the cadmium was calculated and adjusted for the natural abundance of ^{113}Cd. Gamma-induced pair production in platinum and gold foils were simulated, as well as positron transport through those foils. Positron absorption in aerogel was simulated. Total detection of o-Ps decay gammas was calculated by absorption rate of positrons, the o-Ps formation rate, the solid angle of the detector, and the efficiency of the EJ-309 detector for 511 keV gammas from o-Ps annihilations.

The simulated neutron conversion process shows promise for use in difficult neutron detection environments. While the low efficiency prohibits its use in low neutron flux applications, some of the environments this was designed to measure can have a neutron flux of up to 10^{19} neutrons per second per cm^2 [5]. A neutron flux this large would still have an estimated detection rate of 6 X 10^9 annihilation gammas from Ps per second, making this scheme quite viable. As the characterization of the ion acceleration mechanisms in LPI environments is still ongoing [4], additional tools such as this conversion system would help the investigation of these mechanisms.

The delay time of the polyethylene moderation step was calculated to be about 331 μs. This is sevaral orders of magnitude longer than the delay inherent from the ortho-positronium lifetime. These calculations were done with rough estimates of the mean free path of a neutron in PE, and using the lethargy of the dominant hydrogen portion of the PE molecule as a stand in for the lethargy of the material

as a whole. These simplifications have likely induced error into this value. More in-depth calculations will be required using neutron transport modeling such as with MCNP or GEANT4. However, experimental measurement will be used to determine the neutron delay from moderation.

5.1 Future Work

This simulated conversion scheme will be tested in the near future, using the geometry and methods described within. An AmBe source with a weaker neutron production rate of 5 X 10^5 neutrons per second will be used to test the system. With the large delay introduced by the polyethylene moderation, a start signal from the gamma rays produced during neutron capture in the cadmium may be used to determine the positronium lifetime instead of the gammas correlated with the neutron's production. The initial 4.4 MeV gamma produced in the AmBe source would still make a good start signal to experimentally determine the delay imposed by the moderation step. Higher efficiency detectors with slower response times could be employed due to the low activity of the AmBe source during the validation process. Multiple detectors could also be used to increase the solid angle for detection. These improvements could help increase overall detection efficiency, thus decreasing the needed count times.

Validation of this system with decay-based neutron sources will hopefully allow it's use for better measurement of neutron creation through laser-plasma interactions and LPI ion acceleration. Due to the very prompt nature of these interactions and their high neutron flux, faster detectors such as the discussed EJ-309 will be needed in these environments.

As the characterization of these LPI environments progresses, the ability to expand the scope of investigations will similarly progress. Introducing RF signals into these

environments and measuring their interactions could help build understanding as how nuclear event environments will affect RF propagation.

Bibliography

1. McKay Williams William S. Sward, Taylor Swanson. Technical report.

2. F. L. Hill. Technical report.

3. K. D. Fische D. R. Austin G. K. Ngirmang N. R. Murphy C. Orban E. A. Chowdhury J. T. Morrison, S. Feister and W. M. Roquemore. Mev proton acceleration at khz repetition rates from ultra-intense laser liquid interaction. *New Journal of Physics*, pages 1–12, February 2018.

4. D. Henzlova S. Croft K. Falk D. C. Gautier K. D. Ianakiev M. Iliev S. Palaniyappan M. Roth J. C. Fernandez A. Favalli, N. Gular and M. T. Swinhoe. Characterizing laser-plasma ion accelerators driving an intense neutron beam via nuclear signatures. *Nature*, 9(2004), 3019.

5. M. Roth and M. Schollmeier. Ion acceleration - target normal sheath acceleration. pages 23–29, November 2013.

6. H.N. Pendelton S. Berko. Positronium. *Annual Review of Nuclear Particle Science*, 30:543–581, 1980.

7. Kenneth S. Krane. *Introductory Nuclear Physics*. John Wiley and Sons, 1988.

8. P.E. Mallon Y.C. Jean and D.M. Scrader. *Principles and Applications of Positron and Positronium Chemistry*. World Scientific Publishing Co. Pte. Ltd, 2003.

9. Dmitrii S. Zvezhinskiy Silles Duplatre Roman R. Nurmukhamotov Sergey V. Stepanov, Vsevolod M. Brakov and Petr S. Stepanov. Positronium in a liquid phase: Formation, bubble state and chemical reactions. *Advances in Physical Chemistry*, 2012, 2012.

10. S. J. Tao. Positronium annihilation in molecular substances. *Journal of Chemical Physics*, 59(11), June 1972.

11. SelimLab. Tao-eldrup positronium bubble model. http://physics.bgsu.edu/selimlab/tao-eldrup-positronium-bubble-model/, 2019.

12. Ken Wada and Toshio Hyodo. A simple shape-free model for pore size estimation with positron annihilation lifetime spectroscopy. 2013.

13. J. Sampau F. Salvat, J. Fernandez-Vera. A code system for monte carlo simulation of electron and positron transport. OECD/NEA Data Bank (penelope), 2010.

14. Nist xcom database. https://physics.nist.gov/PhysRefData/Xcom/html/xcom1.htmll, 2021.

15. L. Kissel D. E. Cullen, J. H. Hubbell. The evaluated photon data library, '97 version. Technical report, University of California, Lawrence Livermore National Laboratory, 1997.

16. Shawn McTaggart Joshua Machacek and Larry Burggraf. Single-shot positron annihilation lifetime spectroscopy using a liquid scintillator. *AIP Advances*, May 2021.

17. H. K. M. Tanaka D. B. Cassidy, S. H. M. Deng. Single shot positron annihilation lifetime spectroscopy. *Applied Physics Letters*, 88(194105), March 2006.

18. Eljen Technology, https://eljentechnology.com/products/liquid-scintillators/ej-301-ej-309. *Neutron/Gamma PSD EJ-301, EJ-309*, 2021.

19. K. Schreckenbach P. Sperr W. Triftshauser R. Repper C. Hugenschmidt, G. Kogel. First platinum moderated positron beam based on neutron capture. *Nuclear Instruments and Methods in Physics Reseach B*, 198:220–229, 2002.

20. T. Sano H. Kawabe Y. Nagai K. Nagumo K. Inoue T. Toyama N. Oshima A. Kinomura Q. Xu, K. Soto and Y. Shirai. Positron beam facility at kyoto university research reactor. 2014.

21. Louis Schulte. Actinide beryllium neutron source with reduced dispersion characteristics. background information on ambe source fabrication. patent s-116,232. March 2011.

22. R. Nakamura S. Nakayama M. Matsumoto H. Miyamara I. Murata, I. Tsuda. Neutron and gamma-ray source-term characterization of ambe sources in osaka university. *Progress in Nuclear Science and Technology*, 4:345–348, 2014.

23. A.M. Becerra-Ferreiro A. Carrillo-Nunez H.R. Vega-Carrillo, E. Manzanares-Acuna. Neutron and gamma-ray spectra of 239 pube and 241 ambe. *Applied Radiation and Isotopes*, 57:167–170, 2002.

24. Nuclear data center at kaeri. http://atom.kaeri.re.kr/, 2021.

25. Wikipedia. Polyethylene. https://commons.wikimedia.org/w/index.php?curid=1019608, 2021.

26. D. Krstic D. Nikezic, P. K. N. Yu. Characteristics of protons exiting from a polyethylene converter irradiated by neutrons with energies between 1 kev and 10 mev. *PLOS One*, 2016.

27. U.S. Nuclear Regulatory Commission. Neutron sources. https://www.nrc.gov/docs/ML1122/ML11229A704.pdf, 2010.

28. K. I. Roulston R. W. Pringle, H. W. Taylor. Radiative capture of thermal neutrons by cd113. *Physical Review*, 87(6):1016–1017, 1952.

29. Nist x-ray mass attenuation coefficients. https://physics.nist.gov/PhysRefData/XrayMassCoef/tab3 2021.

30. C. Jollet A. Meregaglia A. Minotti S. Perasso A. Tonazzo G. Consolati, D. Franco. A new anti-neutrino detection technique based on positronium tagging with plastic scintillators. *Instruments and Detectors*, 2016.

31. D. Cester G. Nebbia L. Sajo-Bohus G. Viesti F. Pino, L. Stevanato. The light output and detection efficiency of the liquid scintillator ej-309. *Applied Radiation and Isotopes*, 89:79–84, 2014.

REPORT DOCUMENTATION PAGE

Form Approved
OMB No. 0704–0188

1. REPORT DATE *(DD–MM–YYYY)*	2. REPORT TYPE	3. DATES COVERED *(From — To)*
17-06-2021	Master's Thesis	Sept 2019 — Jun 2021

4. TITLE AND SUBTITLE

Neutron Pulse-Time Extension
Through Conversion to Positronium

5a. CONTRACT NUMBER

5b. GRANT NUMBER

5c. PROGRAM ELEMENT NUMBER

6. AUTHOR(S)

McTaggart, Shawn, T

5d. PROJECT NUMBER

5e. TASK NUMBER

5f. WORK UNIT NUMBER

7. PERFORMING ORGANIZATION NAME(S) AND ADDRESS(ES)

Air Force Institute of Technology
Graduate School of Engineering and Management (AFIT/EN)
2950 Hobson Way
WPAFB OH 45433-7765

8. PERFORMING ORGANIZATION REPORT NUMBER

AFIT-ENP-MS-21-J-031

9. SPONSORING / MONITORING AGENCY NAME(S) AND ADDRESS(ES)

AFRL/RIT
Paul F. Gilgallon, Principal Engineer, NC3 Systems and Technology Lead
525 Brooks Road
Rome NY 13441

10. SPONSOR/MONITOR'S ACRONYM(S)

AFRL/RIT

11. SPONSOR/MONITOR'S REPORT NUMBER(S)

12. DISTRIBUTION / AVAILABILITY STATEMENT

DISTRIBUTION STATEMENT A:
APPROVED FOR PUBLIC RELEASE; DISTRIBUTION UNLIMITED.

13. SUPPLEMENTARY NOTES

14. ABSTRACT

Laser-Plasma interactions have strong potential as future neutron sources. Measuring the neutron rate is difficult due to several issues: the very short duration of the laser pulse and subsequent fusion events (on the order of a few picoseconds), the corresponding short duration of the neutron pulse, and the simultaneous emission of other ionizing particles such as protons and electrons. A system was designed to measure neutron emission by imposing a delay from the the emission of other radiation by conversion of the neutrons into ortho-positronium (o-Ps), the triplet state of positronium. This lifetime extension enables more sensitive and selective detection of neutron pulses by time separation of the neutron component from other background signals that are correlated with laser-plasma interactions. Detection of o-Ps annihilation is accomplished with techniques developed for Positron Annihilation Lifetime Spectroscopy (PALS). This research will advance understanding of nuclear processes in laser-plasmas.

15. SUBJECT TERMS
Laser-plasma, neutron, positron, positronium (Ps), ortho-positronium (o-Ps), pair production, positron annihilation lifetime spectroscopy (PALS), single-shot positron annihilation lifetime spectroscopy (SSPALS), pyPenelope simulation, high-altitude nuclear event (HANE)

16. SECURITY CLASSIFICATION OF:			17. LIMITATION OF ABSTRACT	18. NUMBER OF PAGES	19a. NAME OF RESPONSIBLE PERSON
a. REPORT	b. ABSTRACT	c. THIS PAGE			Dr. Larry Burggraf, AFIT/ENP
U	U	U	UU	45	19b. TELEPHONE NUMBER *(include area code)* (937) 255-3636 x4507; larry.burggraf@afit.edu